Journal of Catalysis **208,** 456–466 (2002)
doi:10.1006/jcat.2002.3577

Preparation and ^{31}P NMR Characterization of Nickel Phosphides on Silica

C. Stinner, Z. Tang,[1] M. Haouas,[2] Th. Weber, and R. Prins[3]

Laboratory for Technical Chemistry, Swiss Federal Institute of Technology (ETH), 8093 Zurich, Switzerland

Received December 20, 2001; revised February 18, 2002; accepted February 20, 2002

We prepared Ni_2P by reduction of an oxidic precursor consisting of nickel oxides and phosphates (P/Ni ratio = 0.5) in a flow of H_2 upon heating to 823 K. SiO_2-supported Ni_2P was prepared by reducing a supported oxidic precursor (P/Ni ratio = 0.65) in a flow of 5% H_2/N_2 upon heating to 1023 K. Supported precursors with a P-to-Ni ratio lower than 0.65 yielded phosphides with a lower P content, such as Ni_3P and $Ni_{12}P_5$. Furthermore, the flow rate of the reducing agent has a strong effect on which phosphide forms. From temperature-programmed reduction measurements, we concluded that the reduction starts with the formation of Ni metal from NiO at around 600 K. Phosphates are reduced at higher temperatures to volatile P compounds that react with the Ni to Ni_2P, with Ni_3P and $Ni_{12}P_5$ as possible intermediates. The formed products were characterized by powder X-ray diffractometry and ^{31}P MAS NMR spectroscopy. NMR spectroscopy is a powerful tool for identifying the different Ni phosphides on the support. The metallic character of Ni_3P, $Ni_{12}P_5$, and Ni_2P classifies their large ^{31}P NMR shifts as Knight shifts, which enables them to be distinguished from those of diamagnetic phosphates. © 2002 Elsevier Science (USA)

Key Words: **supported catalysts; reduction; hydrogen; transition-metal phosphides; nickel compounds; MAS NMR; Knight shift.**

1. INTRODUCTION

Catalysts containing metallic nickel are widely used as hydrogenation catalysts (1). By adding elements such as phosphorus or boron, Ni catalysts can be chemically modified (2). This type of modification may lead to the formation of alloys or intermetallic compounds, the structural or electronic properties of which differ from the pure metal (3, 4). Depending on the preparation method, the resulting catalyst contains either an amorphous Ni–P alloy or a nickel phosphide of defined stoichiometry, e.g., Ni_2P.

The phase diagram of nickel and phosphorus is very complex (5). Eleven phases have been reported in the literature with compositions ranging from Ni_3P to NiP_3. In the Ni-rich region of the phase diagram (<40 at% P), the phases Ni_3P, α-Ni_5P_2, γ-$Ni_{12}P_5$, and Ni_2P are reported to be stable up to temperatures between 1173 and 1273 K. The solid solubility of P in Ni is limited and reaches a maximum of 0.32 at% P at 1146 K (5). Up to 25 at% P (=Ni_3P) no thermodynamically stable phases have been reported. However, this compositional range is accessible through the amorphous Ni–P alloys.

Amorphous Ni–P alloys are prepared for the most part by rapid quenching of melts (6) or by a process known as electroless chemical deposition, i.e., the autocatalytic reduction of Ni^{2+} ions by hypophosphite ions $H_2PO_2^-$ (7). Unsupported amorphous Ni–P alloys can be prepared by both methods (8), whereas supported amorphous Ni–P alloys can be prepared by electroless chemical deposition only (9, 10). The amorphous catalysts show an enhanced activity compared with crystalline Ni catalysts (3). However, the amorphous character of the catalysts is an inherent problem. Since these phases are metastable, they tend to crystallize at elevated temperatures, which goes along with sintering and deactivation (10). The crystallization product consists mainly of Ni mixed with Ni_3P since the P content tends to be rather low (<20 at% P) (11).

Preparation methods of stoichiometrically defined crystalline Ni–P compounds include the direct reaction from the elements at high temperatures (12) as well as the reduction of precursors containing nickel phosphates in a flow of H_2 at moderately high temperatures (13). The reduction in H_2 gas has been employed to prepare unsupported as well as supported nickel phosphide catalysts that were tested in hydrogenation and hydrodenitrogenation reactions (14–17). Those catalysts mainly contain Ni_2P as the active component.

Recently, we studied the activity of a number of transition-metal phosphides in the removal of nitrogen (hydrodenitrogenation) from *o*-propylaniline (18). All the tested compounds were active. However, they were unsupported, with the consequence that the surface area was rather low. To increase the active surface area, the dispersion of the phosphides on a high-surface carrier such as γ-Al_2O_3 or SiO_2 is desirable. Among the unsupported transition-metal phosphides, crystalline Ni_2P forms easiest at a fairly low reduction temperature. Therefore, we studied

[1] Current Address: Department of Chemistry, PSI 107, Oklahoma State University, Stillwater, Oklahoma 74078.

[2] Current Address: Laboratoire de Physico-Chimie des Hydrocarbures, UMR 7513, Institut Le Bel, Université Louis Pasteur, 4 rue Blaise Pascal, 67070 Strasbourg Cedex, France.

[3] To whom correspondence should be addressed. Fax: +41 1 632 1162. E-mail: prins@tech.chem.ethz.ch.

0021-9517/02 $35.00

the preparation of Ni_2P on a support. γ-Al_2O_3 is known to react with phosphate to form aluminum phosphates on the surface (19, 20). The formation of aluminum phosphates competes with the formation of phosphides, because the stability of aluminum phosphates toward reduction is very high (19). Therefore, we started with amorphous SiO_2 as the support, which interacts to a lesser extent with phosphates. By adapting the reaction parameters of the reduction in H_2 gas, Ni_2P supported on SiO_2 was prepared and identified by powder X-ray diffraction as well as by ^{31}P MAS NMR spectroscopy.

2. EXPERIMENTAL

2.1. Synthesis

Unsupported Ni_2P was prepared as follows: Diammonium hydrogen phosphate $(NH_4)_2HPO_4$ was dissolved in deionized water, and then a solution of nickel nitrate $Ni(NO_3)_2 \cdot 6H_2O$ was added (all Fluka, puriss. p.a.). The amounts of the nickel salt and phosphate were chosen according to the stoichiometry of the corresponding nickel phosphide, Ni_2P. After evaporation of the water, the obtained solid was calcined in air at 773 K for 5 h and then reduced in a stream of H_2 (99.999%, 300 ml $\cdot$ min^{-1}) at 823 K (14, 15, 17).

Supported phosphides were prepared by pore volume impregnation of a silica support. The silica support (chromatography gel, C-560, CU Chemie Uetikon; surface area, 500 m$^2 \cdot$ g^{-1}; pore volume, 1 ml $\cdot$ g^{-1}) was first ground, sieved (63–90 μm), and then dried for 12 h at 423 K. In a first impregnation step, an aqueous solution of 1.125 M $Ni(NO_3)_2 \cdot 6H_2O$ was added drop by drop to the support. After drying at 423 K for 5 h, an 0.562 M aqueous solution of $(NH_4)_2HPO_4$ was added. The loadings were calculated from the amounts used in the impregnation procedure. The Ni loading of the calcined precursors was 5.9% and the P loading 1.5, 1.7, or 2.0%. After drying at 423 K for 5 h the impregnated support was calcined at 623 K for 5 h. Reduction of the obtained precursor was done at 1023 K (heating rate, 2 K $\cdot$ min^{-1}) in a flow of a 5% H_2/N_2 mixture or in pure H_2 at a flow rate between 10 and 600 ml $\cdot$ min^{-1}. Reduction conditions are summarized in Table 1. Finally, the surface of the samples was passivated in a flow of 0.5% O_2/He (20 ml $\cdot$ min^{-1}) for 2 h at room temperature. The samples prepared in the TPR instrument (see below) were not passivated. The calcined silica-supported samples are designated according to the increasing percentage of P as $NiP_{0.5}$, $NiP_{0.55}$, and $NiP_{0.65}$; the number is the P/Ni atomic ratio.

TABLE 1

Synthesis Conditions for Ni_2P and Supported Samples and the Products as Detected by XRD, Including Their Crystallite Size

Sample	Temperature program[a]	Flow (ml $\cdot$ min^{-1})	Gas	Products[b]	Crystallite size (nm)[c]
Unsupported $NiP_{0.5}$	823	300	H_2	Ni_2P	70
$NiP_{0.5}$	473/723[d]	300	H_2	Ni	10
$NiP_{0.5}$	523/1023	10	5% H_2/N_2	Ni_3P	25
$NiP_{0.5}$	523/1023	50	5% H_2/N_2	$Ni_{12}P_5$	25
$NiP_{0.55}$	523/1023	50	5% H_2/N_2	$Ni_{12}P_5$	30
				Ni_2P	50
$NiP_{0.55}$	523/1023	200	5% H_2/N_2	$Ni_{12}P_5$	30
				Ni_2P	50
$NiP_{0.55}$	523/1023	600	5% H_2/N_2	$Ni_{12}P_5$	30
				Ni_2P	50
$NiP_{0.65}$	523/1023	200	5% H_2/N_2	Ni_2P	45

[a] The temperature was increased from RT to the first indicated temperature (in K) at 2 K $\cdot$ min^{-1} and then to the final temperature at 1 K $\cdot$ min^{-1}. The unsupported $NiP_{0.5}$ sample was heated to 823 K at 1 K $\cdot$ min^{-1}.

[b] Observed by XRD.

[c] According to the Scherrer equation: $d = 0.9\lambda(\beta_{1/2}\cos\theta)^{-1}$, where d = mean crystallite size in nm, λ = X-ray wavelength in nm, $\beta_{1/2}$ = full width at half maximum of a peak in radians, and θ = reflection angle in degrees.

[d] This sample was left at 723 K for 60 min. All the others were left at the final reduction temperature for 15 min.

2.2. Characterization

XRD measurements were carried out with a Siemens D-5000 powder X-ray diffractometer (Cu $K\alpha$ radiation) with Bragg–Brentano geometry. A sample was pressed into a flat-bed sample holder, which was rotated during the measurement. All the patterns were compared with calculated patterns using the software PowderCell 2.3 (21). The single-crystal data of Ni_3P, $Ni_{12}P_5$, and Ni_2P were used as structure input files (22). The PowderCell software facilitates the full pattern fitting of observed powder patterns, and mixtures of crystalline phases can be analyzed in terms of composition. The weight percentage of a phase is given by the ratio of the sum of its integrated intensities and the total intensity of all the phases, taking the densities (as calculated by the PowderCell software) and the cell volumes of all the phases into consideration. The relative errors were estimated to be 10%. The mean crystallite size of a phase was estimated according to the Scherrer equation.

Temperature-programmed reduction (TPR) experiments were carried out with a Micromeritics AutoChem 2910 apparatus. For the measurements, a sample was placed in a quartz U-tube and reduced in a flow of a 4.8% H_2/Ar mixture. ^{31}P NMR spectra were obtained with an Advance 400 WB Bruker spectrometer equipped with a magic-angle-spinning probe. The ^{31}P NMR frequency was 161.9 MHz and 85% phosphoric acid was used as an external reference. Samples were ground; in the case of the unsupported Ni_2P they were mixed with 50 wt% of pure silica powder to provide electrical insulation between the metallic particles and, thus, to avoid the appearance of eddy currents within the sample. The resulting samples were packed in a

4-mm-diameter rotor and spun at 10–15 kHz. The spectra were obtained by Fourier transforming the free induction decay signals. Spectra were acquired using a single 1.8-μs pulse causing a flip angle of about $\pi/4$ and a recycle time of 1 s. The measurements were performed at room temperature with 1800 scans. The ^{31}P shift anisotropy was determined from the spinning sideband intensities in the MAS spectra (23). Spectra were simulated using a modified version of the Bruker Winfit program (24).

3. RESULTS

3.1. Preparation of Unsupported Ni_2P

The preparation of unsupported dinickel phosphide, Ni_2P, by reduction in flowing H_2 gas is straightforward (14, 15). An appropriate amount of an aqueous solution of $Ni(NO_3)_2 \cdot 6H_2O$ was added to an aqueous solution of $(NH_4)_2HPO_4$ so that a mixture results containing nickel and phosphorus in a ratio of 2:1. Upon addition of the nickel-containing solution a light green precipitate was formed that contained different nickel phosphates, e.g., $Ni_3(PO_4)_2 \cdot 8H_2O$ or $(NH_4)NiPO_4 \cdot H_2O$, as reported in the literature (25). Upon drying and calcination volatile compounds such as H_2O, NH_3, and nitrous gases were expelled. The resulting light brown solid consisted of NiO (from XRD results, not shown here) and nickel phosphates of different composition (from Raman measurements, not shown here). Nevertheless, from this heterogeneous mixture only Ni_2P formed upon reduction in a flow of H_2 gas while heating to 823 K at a heating rate of 1 K $\cdot$ min^{-1}, since no other phases were detected in the XRD powder pattern (Fig. 1). However, the preparation of Ni_2P supported on amorphous silica was more complicated.

3.2. Preparation of Supported Nickel Phosphides

Oxidic precursors of supported nickel phosphides were prepared by pore volume impregnation. Two impregnation steps were necessary to introduce Ni and P onto the SiO_2 support, because in a one-step impregnation an insoluble precipitate of nickel phosphate forms on mixing aqueous solutions of $Ni(NO_3)_2 \cdot 6H_2O$ and $(NH_4)_2HPO_4$, as described above for the unsupported Ni_2P. The impregnation was started with the $Ni(NO_3)_2 \cdot 6H_2O$ solution to achieve good dispersion of the Ni^{2+} cations on the SiO_2 surface. After an intermediate drying step the $(NH_4)_2HPO_4$ solution was added to the support. Further drying and calcination at 623 K yielded the supported precursor.

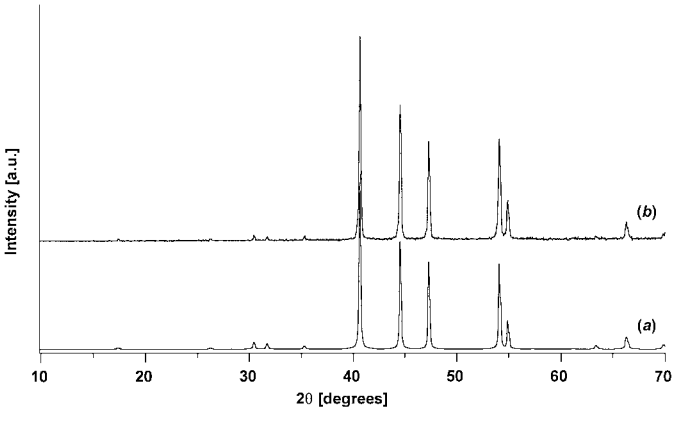

FIG. 1. XRD powder patterns of unsupported Ni_2P: calculated (a) and observed (b).

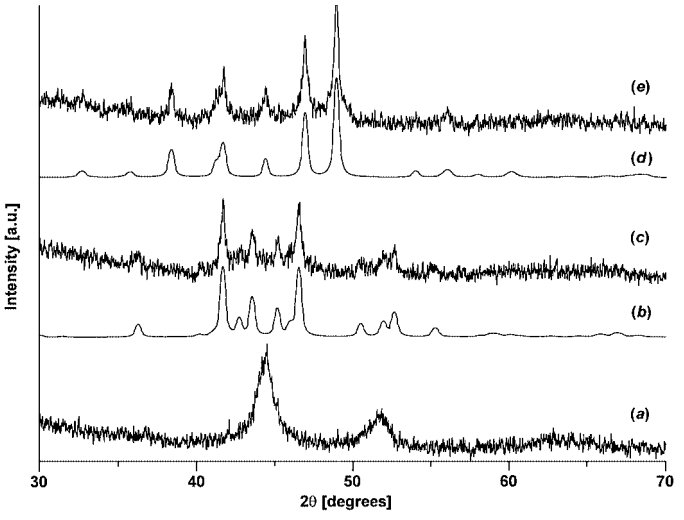

FIG. 2. Observed XRD powder patterns of the sample $NiP_{0.5}$ reduced at different flow rates and temperatures: (a) 300 ml $\cdot$ min^{-1} H_2/723 K, (c) 10 ml $\cdot$ min^{-1} 5% H_2/N_2/1023 K, (e) 50 ml $\cdot$ min^{-1} 5% H_2/N_2/1023 K; calculated patterns of (b) Ni_3P and (d) $Ni_{12}P_5$.

When the $NiP_{0.5}$ precursor was reduced in pure H_2 gas at 723 K, no Ni_2P was detected in the XRD pattern. Only cubic Ni metal was formed (Fig. 2a). To determine whether phosphate was still present, we measured the TPR profile of the reduced and passivated $NiP_{0.5}$ sample up to 1023 K (Fig. 3a). In the TPR profile, only one signal, at 367 K, was observed, which can be attributed to the reduction of (surface) Ni oxide formed during or after the passivation. The consumption of H_2 showed that about 30% of the Ni was present as Ni^{2+}. No further signal was detected up to 1023 K.

When we performed a TPR experiment on the oxidic $NiP_{0.5}$ precursor, we observed a TPR profile with two maxima around 610 and 830 K and a shoulder around 880 K (Fig. 3b). The sample contained 128 μmol of Ni^{2+} and 64 μmol of phosphate species with P in the oxidation state of 5+. If Ni^{2+} and P^{5+} are reduced to Ni^0 and P^0, then a total H_2 consumption of 288 μmol is expected. The experimentally observed peak areas correspond to a H_2 consumption of 300 μmol, in agreement with the theoretically expected value within the experimental error of 10%.

Figure 3c shows the TPR profile of the unsupported $NiP_{0.5}$ precursor. The reduction started at about 600 K and

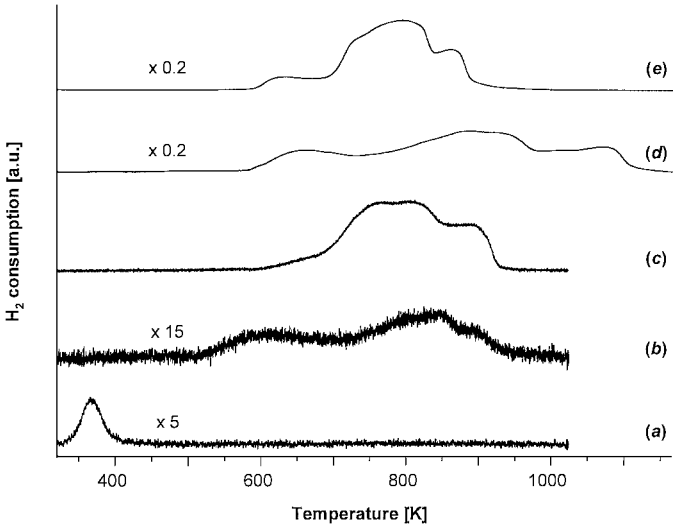

FIG. 3. TPR profiles of (a) $NiP_{0.5}$ (after reduction at 723 K in 300 ml · ml^{-1} H_2 for 1 h and passivation), (b) the oxidic $NiP_{0.5}$ precursor (1023 K, 2 K · min^{-1}, 50 ml · min^{-1} 4.8% H_2/Ar), (c) the unsupported oxidic $NiP_{0.5}$ precursor (1023 K, 10 K · min^{-1}, 50 ml · min^{-1} 4.8% H_2/Ar), (d) the oxidic $NiP_{0.5}$ precursor (1173 K, 5 K · min^{-1}, 10 ml · min^{-1} 4.8% H_2/Ar), and (e) the unsupported oxidic $NiP_{0.5}$ precursor (1173 K, 5 K · min^{-1}, 10 ml · min^{-1} 4.8% H_2/Ar).

was finished at about 920 K. The H_2 consumption corresponded to a complete reduction to Ni_2P. The sample contained 380 μmol of Ni^{2+} and 190 μmol of phosphate species with P in an oxidation state of 5+. Thus, the expected total H_2 consumption is 855 μmol of H_2, which is in good agreement with the experimentally observed value of 882 μmol of H_2. Four features can be distinguished in this TPR profile: a shoulder at 660 K; two large peaks, with maxima around 750 and 820 K; and a smaller peak at 890 K. A comparison with the TPR profile of the supported $NiP_{0.5}$ sample shows that the support has a strong influence on the reduction behavior. The TPR results show that the reduction of supported $NiP_{0.5}$ was complete around 930 K. Therefore, we performed subsequent reductions up to 1023 K.

The increase in temperature led to the formation of different Ni phosphides. The type of Ni phosphide that formed depended strongly on the gas flow rate. With a low flow rate, Ni_3P formed (Fig. 2c), and in the 2θ range from 40 to 48° a broad reflection was present underneath the reflections of Ni_3P. When the flow rate of the reducing agent was increased to 50 ml · min^{-1}, the formation of $Ni_{12}P_5$ was observed (Fig. 2e). Nevertheless, we were not able to obtain the desired Ni_2P product. Therefore, we increased the amount of phosphate in the precursor relative to Ni. If a reactive P species forms in the gas phase and reacts with the Ni, then an increase in the concentration of this volatile species might have a beneficial effect on the P content of the eventual nickel phosphide.

Figures 4a–4c show the XRD patterns of the materials obtained from the oxidic $NiP_{0.55}$ precursor after reduction to 1023 K in 5% H_2/N_2 at a flow rate between 50 and 600 ml · min^{-1}. All three samples contain a mixture of Ni_2P and $Ni_{12}P_5$. The Ni_2P-to-$Ni_{12}P_5$ ratio increased as the flow rate increased. The samples obtained for flow rates of 200 and 600 ml · min^{-1} had more or less the same composition and contained 80% Ni_2P and 20% $Ni_{12}P_5$, whereas the sample obtained at 50 ml · min^{-1} contained 50% Ni_2P and 50% $Ni_{12}P_5$. Ni_2P was the only phosphide obtained with the $NiP_{0.65}$ precursor with an even higher P content than the other precursors in combination with the sufficiently high flow rate of 200 ml · min^{-1} (Fig. 4d). According to the estimated crystallite sizes given in Table 1, all supported samples contain nickel phosphide particles that are smaller than those of the unsupported Ni_2P sample.

The influence of the flow rate on the reduction behavior was also observed in the TPR profiles of the supported and unsupported $NiP_{0.5}$ samples (Figs. 3d and 3e). Compared with the results shown in Fig. 3b, the influence of the lower flow rate on the TPR profile of the supported $NiP_{0.5}$ sample can be clearly seen (Fig. 3d). The reduction begins at 600 K and is finished at around 1100 K. The overall shape of the two profiles is very similar, but all the maxima are shifted toward higher temperatures (660, 880, 930, and 1080 K) and the profile is stretched. On the other hand, the TPR profile of unsupported $NiP_{0.5}$ was barely affected by a lower flow rate. The reduction started at 580 K and was finished at 900 K.

3.3. ^{31}P MAS NMR Results

Phosphorus contains only one isotope, ^{31}P, with a nuclear spin of $I = 1/2$. This and the high magnetic moment (which results in a high sensitivity) make it an interesting nucleus for NMR spectroscopy. Solid state NMR gives insight into the structure of solids and enables us to probe the local

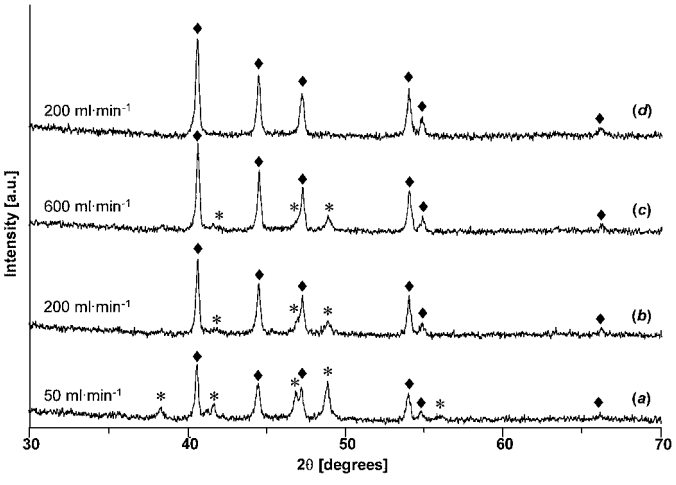

FIG. 4. Observed XRD powder patterns of the samples $NiP_{0.55}$ (a–c), and $NiP_{0.65}$ (d) reduced to 1023 K in a flow of 5% N_2/H_2 at the flow rates indicated. ∗, $Ni_{12}P_5$; ◆, Ni_2P.

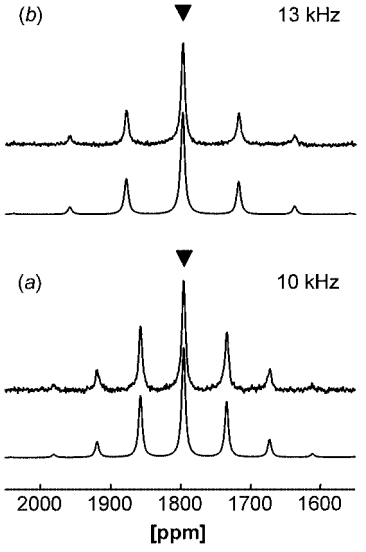

FIG. 5. ^{31}P MAS NMR spectra of Ni_3P/SiO_2 ($NiP_{0.5}$; 10 ml · min^{-1} 5% H_2/N_2, 1023 K) at two different spinning rates (a, 10 kHz; b, 13 kHz). Centerbands are indicated by triangles. Simulated NMR spectra are displayed below each trace.

environment of a nucleus. Unlike X-ray diffraction, NMR spectroscopy is not restricted to materials with long-range order but can also be applied to amorphous substances. In our samples, phosphorus is present as crystalline phosphides and in the form of phosphates. As a first step, we wanted to find out whether ^{31}P MAS NMR distinguishes between the different species. On the basis of our XRD results, we measured the ^{31}P MAS NMR spectra of those samples that contained crystalline Ni phosphides (Ni_3P, $Ni_{12}P_5$, Ni_2P). The observed spectra are shown in Figs. 5–7.

The NMR shift range from +500 to +5000 ppm revealed only one sideband pattern with an isotropic chemical shift of 1797 ± 5 ppm for the $NiP_{0.5}$ sample containing Ni_3P supported on SiO_2 (Fig. 5). The spectra of all the measured phosphides showed strong distortions of the baseline, and first-order phase corrections were necessary in most cases. Using the Winfit software, the centerband with the sideband pattern was fitted according to the method of Herzfeld and Berger (23). Table 2 presents the values of the fitted parameters (isotropic chemical shift δ_{iso}, chemical shift anisotropy δ_{CSA}, asymmetry parameter η), which describe the chemical shift anisotropy, as well as the observed linewidths for all the reported spectra.

Figure 6 shows the two sideband patterns that were observed at each of two different spinning rates for the $NiP_{0.5}$ sample that contained $Ni_{12}P_5$ supported on SiO_2. The isotropic chemical shifts were 1940 and 2262 ± 5 ppm. The fitted spectra are plotted below the experimental spectra. Two sideband patterns were observed for the unsupported Ni_2P as well as for the Ni_2P supported on SiO_2. Figure 7 shows the spectra obtained for both materials at a spinning rate of 10 kHz. The isotropic chemical shifts are 1487

TABLE 2

^{31}P MAS NMR Results

Sample	ν_{rot} (kHz)	δ^a_{iso} (ppm)	FWHM^b (kHz)	δ^a_{CSA} (ppm)	η^a
Ni_3P/SiO_2	10	1796	1.0	−135	0.9
Ni_3P/SiO_2	13	1798	1.0	−136	0.9
$Ni_{12}P_5/SiO_2$	10	1941	1.8	173	0.1
		2259	1.4	241	0.4
$Ni_{12}P_5/SiO_2$	13	1938	1.8	168	0.1
		2264	1.3	241	0.4
Ni_2P/SiO_2	10	1487	1.0	−271	0
		4081	2.5	−73	0.85
Ni_2P	10	1487	1.2	−284	0.55
		4076	4.1	120	0.7

[a] δ_{iso}, δ_{CSA}, and η are defined by the principal elements (δ_{ii}) of the chemical shift tensor as $\delta_{iso} = 1/3(\delta_{11} + \delta_{22} + \delta_{33})$; $\delta_{CSA} = \delta_{33} - \delta_{iso}$; $\eta = (\delta_{22} - \delta_{11})/(\delta_{33} - \delta_{iso})$ with $|\delta_{33} - \delta_{iso}| \geq |\delta_{11} - \delta_{iso}| \geq |\delta_{22} - \delta_{iso}|$.
[b] Full width at half maximum.

and 4081 ppm (supported) and 1487 and 4076 ppm (unsupported). The relative intensities of the sideband pattern of unsupported Ni_2P at 1487 ppm differs significantly from those of supported Ni_2P, as indicated by the asymmetry parameter $\eta = 0$ for the supported Ni_2P and $\eta = 0.55$ for the unsupported Ni_2P. Other samples containing supported

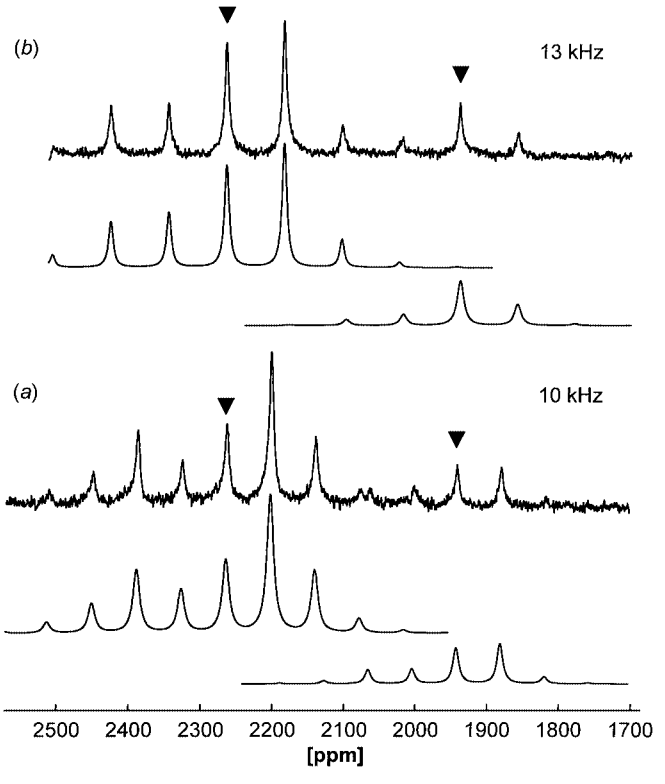

FIG. 6. ^{31}P MAS NMR spectra of $Ni_{12}P_5/SiO_2$ ($NiP_{0.5}$; 50 ml · min^{-1} 5% H_2/N_2, 1023 K) at two different spinning rates (a, 10 kHz; b, 13 kHz). Centerbands are indicated by triangles. Simulated NMR spectra are displayed below each trace.

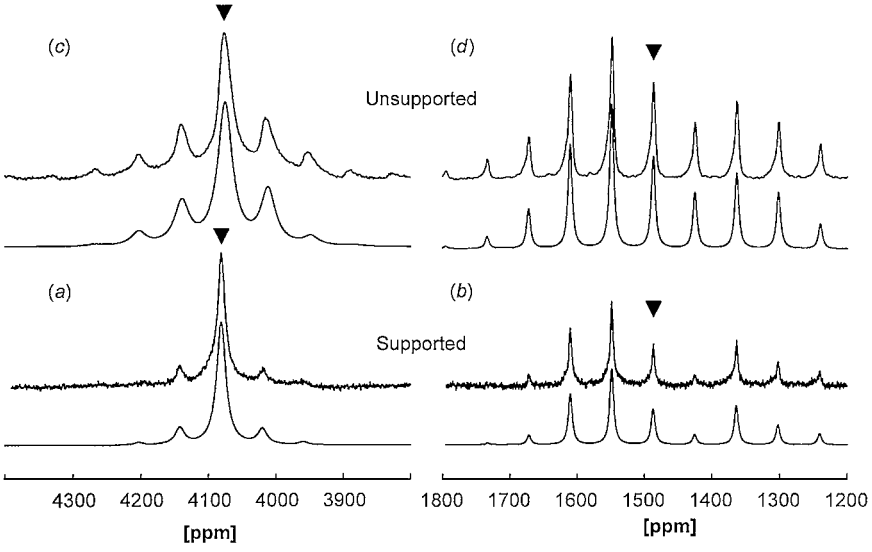

FIG. 7. ^{31}P MAS NMR spectra of (a, b) Ni_2P/SiO_2 ($NiP_{0.65}$; 200 ml · min^{-1} 5% H_2/N_2, 1023 K) and (c, d) unsupported Ni_2P at a spinning rate of 10 kHz. Centerbands are indicated by triangles. Simulated NMR spectra are displayed below each trace.

Ni_2P yielded asymmetry parameter values between 0 and 0.1. The sideband pattern around the band at 4081 ppm was also detected for the other supported Ni_2P samples. However, in unsupported Ni_2P, the centerband of the respective pattern is shifted to 4076 ppm, and the fitting gives a different chemical shift anisotropy as well a slightly different value for η. Especially in the case of the unsupported Ni_2P a large linewidth caused a strong overlap of the bands so that the baseline was not well-defined (Fig. 7c).

No further signals were detected in the unsupported Ni_2P. In all the supported samples, additional peaks were detected in the region around and below 0 ppm. Three peaks, at around +2, −8, and −21 ppm, typical of phosphate species such as $H_nPO_4^{(3-n)-}$, $P_2O_7^{4-}$, and $(PO_3^-)_n$, were usually detected (26, 27). No signals were detected below −30 ppm, indicating that no silicon phosphates were formed (characterized by chemical shifts from −30 to −50 ppm) (28).

4. DISCUSSION

All the TPR profiles have a small peak in common between 600 and 660 K (Fig. 3), which is attributed to the reduction of NiO (29). NiO should be present in all the samples because of the surplus Ni^{2+} compared with the amount of phosphate that is present as PO_4^{3-}, $P_2O_7^{4-}$, or $(PO_3^-)_n$ after calcination (25, 30). For instance, if one assumes that the phosphate species present after calcination is diphosphate $P_2O_7^{4-}$, then two Ni^{2+} ions will be sufficient to compensate for the negative charge of the diphosphate anions. Since the atomic ratio Ni/P is 2 : 1, 50% of the Ni^{2+} ions must compensate for their charges by O^{2-} ions or hydroxyl species from the aqueous impregnation solution or from the silica surface. Louis *et al.* detected NiO, $Ni(OH)_2$, and nickel phyllosilicates on SiO_2 samples impregnated with a $Ni(NO_3)_2 \cdot 6H_2O$ solution (31). They also observed that most of the H_2 consumption for a SiO_2-supported Ni sample, prepared in a manner similar to ours, occurred at around 653 K. This would explain why Ni was detected as the only crystalline phase in the sample that was reduced at 723 K (Figs. 2a and 3a), because the reduction temperature was high enough to reduce NiO but not phosphate. It is not clear why H_2 consumption in the TPR of the reduced and passivated $NiP_{0.5}$ sample was not observed at higher temperatures. Only Ni was detected by XRD, so it is assumed that phosphate is still present. The fact that H_2 consumption was not observed at higher temperatures (Fig. 3a) implies either that no phosphate was left on the support or that some of the phosphate reacted with the SiO_2 surface to silicon phosphates, which may be highly stable against reduction. Krawietz *et al.* reported the formation of silicon phosphates, e.g., $Si_5O(PO_4)_6$, SiP_2O_7, and $SiHP_3O_{10}$, in a study of solid phosphoric acid catalysts prepared by impregnating SiO_2 with H_3PO_4 followed by calcination (28). Assuming that the formed Ni acts as a hydrogenation catalyst, then it is not unlikely that phosphate is no longer present after reduction. A temperature of 723 K would be high enough to catalyze the reduction of the phosphate to volatile P species such as phosphines P_xH_y but would be too low for the formed P_xH_y to react with Ni metal to a phosphide. Since the TPR profiles of the precursors show considerable consumption of H_2 at higher temperatures, we conclude that a minimum temperature is necessary for the reduction as well as for the formation of nickel phosphides.

The H_2 concentration may also have an effect on the reduction behavior. A higher H_2 concentration would lead to

a higher reaction rate for a reaction that has a positive order in H_2. The use of pure H_2 might cause local heating and sintering of the precursor particles. Bigger particles are harder to reduce since the H_2 must diffuse into the bulk and the formed water must leave the bulk. Therefore, we diluted the H_2 as in the TPR experiments. In the case of supported molybdenum and iron oxides, H_2/N_2 gas mixtures may lead to the formation of nitrides. However, it has been reported that Ni nitrides are not stable in the presence of H_2 above 440 K (32, 33).

Not only the composition of the reduction gas but also the flow rate has a strong effect on the reduction behavior of supported catalysts. The reason is that upon reduction, water forms from the oxidic Ni and phosphate species and the pores of the support hinder the diffusion of the H_2O. The higher the vapor pressure of H_2O within the pores, the more the equilibria are shifted to the side of the oxidic Ni and phosphate species:

$$\begin{aligned} \mathrm{NiO} + \mathrm{H_2} &\leftrightharpoons \mathrm{Ni} + \mathrm{H_2O}, \\ \mathrm{P_2O_5} + 5\mathrm{H_2} &\leftrightharpoons \mathrm{P_2} + 5\mathrm{H_2O}, \\ \text{or}\quad \mathrm{P}_x\mathrm{O}_y^{(2y-5x)-} + 2.5x\mathrm{H_2} &\leftrightharpoons x/2\mathrm{P_2} + (5x-y)\mathrm{H_2O} \\ &\quad + (2y-5x)\mathrm{OH}^-. \end{aligned}$$

The influence of the flow rate on the reduction rate was clearly demonstrated by Burratin *et al.* when they studied the product properties of SiO_2-supported Ni obtained by reduction in H_2/Ar (34). They concluded that an increase in the flow rate facilitates the quicker removal of the water formed upon reduction. This shifts the maximum of the reduction to lower temperatures. In addition, they found that the formed Ni particles are smaller, because the removal of water diminishes the sintering of the NiO particles of the precursor. This holds for the reduction of all supported oxidic systems when H_2O forms. This is shown clearly by comparing Figs. 3b and 3c with Figs. 3d and 3e. The unsupported $NiP_{0.5}$ samples are hardly influenced by the flow rate, whereas the temperature maxima of the supported samples shift to higher values at a lower flow rate. The higher reduction rate as well as the formation of smaller particles in our system indicates that more-volatile P species are formed at a higher rate, and diffuse more easily into the Ni particles.

The exact reduction product of phosphate in our reaction is not known, but the reduction must proceed in several steps and volatile species such as elemental P (P_4) or phosphines P_xH_y are probably formed. At higher temperatures, thermodynamics predict that elemental phosphorus is present in the form of P_4 molecules in equilibrium with P_2 molecules (35). Phosphines P_xH_y decompose at higher temperatures to elemental P and H_2. This decomposition may be catalyzed by Ni particles that are formed first; Ryndin *et al.* observed that Ni particles on alumina decompose $AsPh_3$ to benzene and As (36). The formed As reacted at pressures of 6–40 bar and temperatures of 423–473 K with the Ni particles but not with the support and formed NiAs. If a temperature of 423–473 K is sufficient for As to diffuse into Ni particles, then it should be possible for P to react with Ni.

In the case of amorphous Ni–P alloys supported on SiO_2, Li *et al.* showed that a broad signal around 45° 2θ in the XRD pattern corresponds to an amorphous Ni–P phase (10). Their samples were prepared by electroless plating and contained less than 25 at% P, lower than the P content in our samples. After annealing at higher temperatures, they did not observe any formation of Ni_3P below 873 K. However, in an earlier publication the same group reported the detection of Ni_3P after an oxidation-reduction cycle of an unsupported amorphous Ni–P alloy (20 at% P) at 553 K (11). We conclude that the higher P content of our samples and the proposed formation of reactive P species in the gas phase lead to the formation of Ni_3P in our sample.

The reaction of P with Ni proceeds through a sequence of intermediates, the first being Ni_3P. In the Ni–P phase diagram, Ni_3P is the Ni phosphide with the lowest P content close to Ni metal (35). From the phase diagram, Ni_5P_2 is expected to form if the P content is increased. However, we detected $Ni_{12}P_5$, but not Ni_5P_2. The structure and chemistry of Ni_5P_2 are not fully understood. A phase of the composition Ni_5P_2 was first described by Konstantinow, who observed a low-temperature and a high-temperature modification (37). Nowotny and Henglein confirmed the existence of Ni_5P_2 by XRD (38). Neither Saini *et al.* (39) nor Larsson (22) were able to determine the crystal structure of this phase. Furthermore, Larsson corrected the composition of the Ni_5P_2 phase in his study to $Ni_{2.55}P$. Other authors detected Ni_5P_2 when they annealed amorphous Ni–P alloys (40). Pittermann and Ripper found that the P content of electrodeposited Ni–P alloys determines which crystalline Ni phases form upon heating. They detected the formation of Ni and Ni_3P for alloys with P contents below 20 at% and the formation of Ni_5P_2 for P contents between 20 and 29 at%. The Ni_5P_2 phase was metastable, however, and decomposed to Ni_3P and $Ni_{12}P_5$ at 930 K. For even higher P contents, the amorphous phase transformed directly to mixtures of $Ni_{12}P_5$ and Ni_2P. Other authors reported that Ni_5P_2 has a large homogeneity range (5). All these reports indicate that a phase with a composition close to Ni_5P_2 probably exists, but that the thermodynamic stability range of this phase is not clear. Metastable Ni_5P_2, as observed by Pittermann and Ripper, may also have formed during the reduction of our samples, but its thermal lability may have hindered us from detecting it.

Rundqvist and Larsson showed that the structures of Ni_3P and $Ni_{12}P_5$ are very similar (Figs. 8 and 9) (41). Both phosphides crystallize in a tetragonal structure with similar lattice constants (Table 3). The unit cell of Ni_3P contains eight formula units, i.e., 24 Ni and 8 P atoms, whereas the unit cell of $Ni_{12}P_5$ contains two formula units, i.e., 24 Ni atoms and 10 P atoms. The Ni_3P structure has P atoms

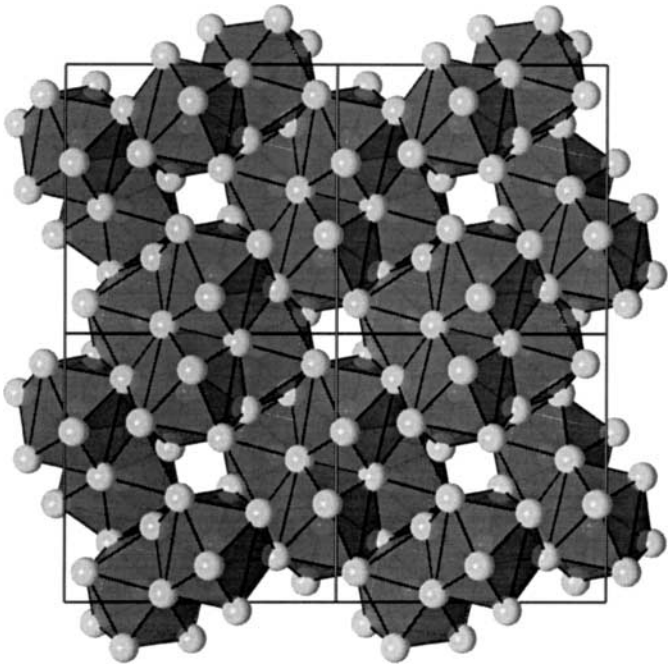

FIG. 8. Projection of the Ni_3P structure along the c axis (2×2 unit cells). Atoms outside the lines indicating the cell edges were added to emphasize the structure motif. Ni atoms are presented as spheres located at the corners of polyhedra formed around the P atoms.

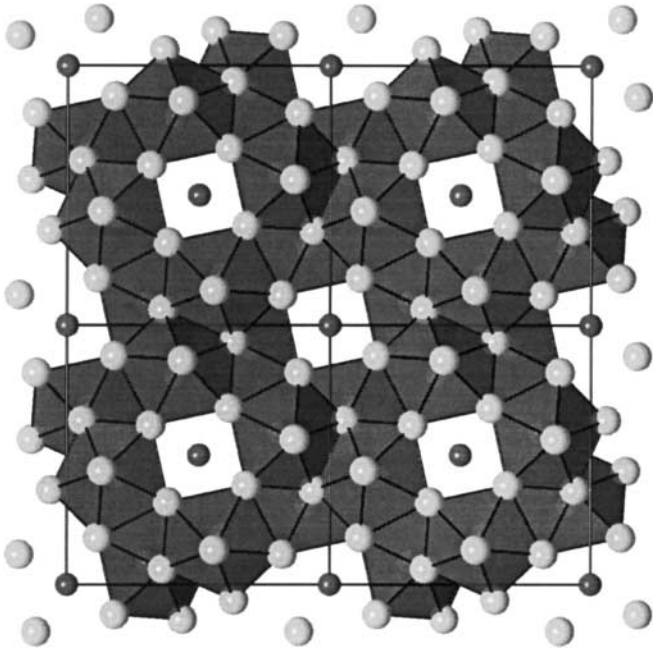

FIG. 9. Projection of the $Ni_{12}P_5$ structure along the c axix (2×2 unit cells). Atoms outside the lines indicating the cell edges were added to emphasize the structure motif. Ni atoms are presented as gray spheres located at the corners of polyhedra formed around the P atoms on 8*h* sites. P atoms at the 2*a* sites are shown as dark gray spheres.

TABLE 3

Crystallographic Data of the Phosphides

Compound	Structure type	Space group[a]	Z[b]	Lattice constants (Å)[c]
Ni_3P	Fe_3P	82 ($I\bar{4}$)	8	$a = b = 8.954$, $c = 4.386$
$Ni_{12}P_5$	$Ni_{12}P_5$	87 ($I4/m$)	2	$a = b = 8.646$, $c = 5.070$
Ni_2P	Fe_2P	189 ($P\bar{6}2m$)	3	$a = b = 5.859$, $c = 3.382$; $\gamma = 120°$

[a] Space group number and short Hermann–Mauguin symbol according to the International Tables for Crystallography.
[b] Formula units per unit cell.
[c] Angles are given only when they deviate from 90°.

on only one crystallographic site and each P atom is coordinated by nine Ni atoms that form a distorted tricapped trigonal prism (Table 4). The two sites in $Ni_{12}P_5$ have coordination numbers of 10 and 8 (Table 4). The 10 Ni atoms form an irregular polyhedron, whereas the eight Ni atoms are located on the corners of a cube. This cubic coordination is clearly seen in the projection of the $Ni_{12}P_5$ structure at the centers and corners of the unit cells (Fig. 9). The occupation ratio of the two P sites in $Ni_{12}P_5$ is four, as given by the ratio of the sites' multiplicities (Table 4). Again comparing $Ni_{12}P_5$ and Ni_3P (=$Ni_{12}P_4$), $Ni_{12}P_5$ has an additional P atom, which is located at the cubic site. A comparison of the structures of Ni_3P with $Ni_{12}P_5$ reveals empty channels in Ni_3P, whereas in $Ni_{12}P_5$ they are filled with the cubic P sites (Fig. 9). The channels in Ni_3P are rather narrow but can be widened by small displacements of some of the Ni atoms, so that the cubic sites of the $Ni_{12}P_5$ structure form. Although Ni_3P and $Ni_{12}P_5$ do not share a direct boundary in the phase diagram, it is likely that a kinetically controlled transformation from

TABLE 4

Site Symmetries and P–M Distances in the Local Environment of P Atoms

Compound	Atom	Position[a]	Distances P–M (Å)
Ni_2P	P(1)	$2c(\bar{6})$	3×2.21
			6×2.46
	P(2)	$1b(\bar{6}2m)$	6×2.27
			3×2.37
$Ni_{12}P_5$	P(1)	$8h(m)$	4×2.23–2.24
			2×2.43
			2×2.46
			2×2.60
	P(2)	$2a(4/m)$	8×2.25
Ni_3P	P	$8g(1)$	2×2.21
			3×2.28–2.29
			4×2.32–2.34

[a] Number and letter refer to the multiplicity and Wyckoff letter of the respective crystallographic position. The site symmetry of the crystallographic position (Hermann–Mauguin notation) is given in parentheses.

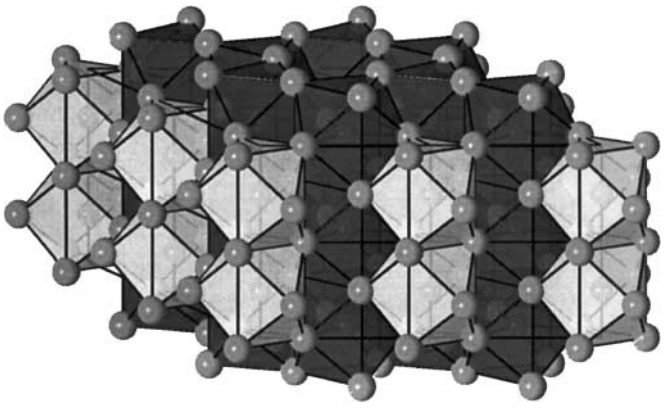

FIG. 10. Ni_2P structure ($3 \times 3 \times 2$ unit cells). Atoms outside the lines indicating the cell edges were added to emphasize the structure motif. Ni atoms are presented as light gray spheres located at the corners of polyhedra formed around the P atoms. Polyhedra around P atoms on 2*c* sites are dark gray; polyhedra around P atoms on 1*b* sites are light gray.

Ni_3P to $Ni_{12}P_5$ takes place when P atoms diffuse into the empty channels of the Ni_3P structure.

$Ni_{12}P_5$ forms a direct phase boundary with Ni_2P up to high temperatures (35). When Ni_2P is written as $Ni_{12}P_6$, it is obvious that the introduction of another P atom into $Ni_{12}P_5$ gives the correct composition. However, the structure of Ni_2P differs considerably from that of $Ni_{12}P_5$. The Ni_2P structure can be visualized as being made up of building blocks of two different tricapped trigonal prisms that form stacks. The stacks are connected by sharing edges and faces with the surrounding stacks (Fig. 10). The large differences between the two structures make a complete rearrangement of the Ni and P atoms necessary. This may explain why the formation of Ni_2P is difficult in the supported materials if $Ni_{12}P_5$ forms first. If $Ni_{12}P_5$ does not form, however, then the direct formation of Ni_2P from Ni or Ni_3P and P is easily accomplished, as seen for the unsupported $NiP_{0.5}$, where no phase other than Ni_2P was detected (Fig. 1). The fact that only Ni_2P forms from the unsupported precursor may be due to the more homogeneous distribution of Ni and P when Ni_2P is prepared in one step. The two-step preparation of the supported precursor and the strong interaction of Ni^{2+} ions with the SiO_2 surface might lead to the segregation of the Ni and phosphate species. As can be seen from the TPR measurements at high flow rate, the reduction of the supported and unsupported $NiP_{0.5}$ precursors starts at different temperatures, 520 and 600 K, respectively, but is complete at about the same temperature (Figs. 3b and 3c). However, the relative H_2 consumption of the first peak is higher for the supported $NiP_{0.5}$. The supported sample contains smaller NiO particles, which start to reduce at around 520 K, whereas the surface reduction of bigger, unsupported NiO particles starts at around 600 K. Alternatively, more NiO may be present in the supported sample than in the unsupported sample, with the consequence that in the supported sample Ni^{2+} and phosphate ions are more separated. The increased segregation may be another reason that Ni_2P does not form easily on the support. The reactive P compounds must diffuse to the Ni particles to react with them.

The crystal structures of Ni_3P, $Ni_{12}P_5$, and Ni_2P have been published (22, 41, 42), and site symmetries of the P atoms and P–M distances are listed in Table 4. As described above, the structures of the three phosphides differ, and the Ni_3P structure contains one crystallographic P site, whereas in the structures of Ni_2P and $Ni_{12}P_5$ two P sites are distinguishable. As a consequence, one signal is observed in Ni_3P and two NMR signals are observed in Ni_2P and $Ni_{12}P_5$ (Fig. 11). The three Ni phosphides belong to the metal-rich phosphides. Metal-rich phosphides usually have metallic character (43–45) and their metal–metal distances are usually close to those of the pure metal (43). The shortest metal–metal distances in Ni_3P, $Ni_{12}P_5$, and Ni_2P are 2.44, 2.53, and 2.61 Å, respectively, while the shortest M–M distance in Ni metal is 2.49 Å. The short M–M distances imply strong metal bonding, which should result in metallic properties such as metallic conductivity. This was confirmed for Ni_2P by Shirotani *et al.* (46). The magnetic susceptibility of Ni_2P, Ni_3P, and other Ni phosphides hardly depends on temperature; thus, these materials are classified as Pauli paramagnets, which provides further evidence of their metallic character (46, 47).

The metallic character of the Ni phosphides explains why the observed NMR shifts are so high (Table 2). In

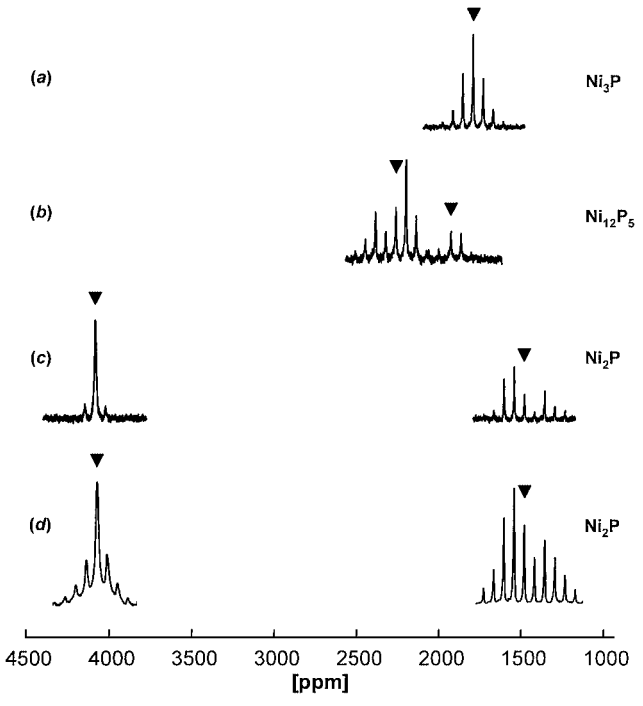

FIG. 11. Overview of the observed ^{31}P MAS NMR spectra of (a) Ni_3P/SiO_2, (b)$Ni_{12}P_5/SiO_2$, (c) Ni_2P/SiO_2, and (d) unsupported Ni_2P.

diamagnetic phosphorus compounds, the shifts are in the range of 200 to −500 ppm (44). The shift in metals is one order of magnitude larger than that in diamagnetic compounds (48). This so-called Knight shift is caused by the density of unpaired conduction electrons at the position of the NMR-observed nuclei in metallic compounds (48). It is difficult to measure Knight shifts in powders accurately, because in addition to the dipolar broadening, susceptibility broadening is also observed (49). The application of magic-angle spinning (MAS) eliminates the dipolar broadening and partly suppresses the effect of the susceptibility broadening if the spinning rate is sufficiently high (50).

A large number of ^{31}P MAS NMR studies on insulating and semiconducting phosphides have been published (51–54), but only few MAS NMR studies are on alloys such as transition-metal phosphides. To the best of our knowledge, Ni_3P is the only Ni phosphide that has been characterized by ^{31}P MAS NMR (55). Furo *et al.* reported an average Knight shift of 1790 ppm for Ni_3P, which is close to our value. In the Ni_2P structure, two different crystallographic P sites are present and, thus, two NMR signals are observed. The relative occurrence of the two sites should be reflected in the ratio of their signal intensities. The ratio between the intensities of the sideband pattern at around 4078 ppm and that at 1487 ppm is around 1.6 ± 0.2 for the unsupported as well as the supported Ni_2P samples, which is in moderate agreement with the expected value of two. Effects due to the paramagnetic nature of the samples might explain the deviation (see below). The electronic properties must be very different at the two P sites because the difference between the Knight shifts is very large in Ni_2P. In $Ni_{12}P_5$ the difference is much smaller but large enough to observe two signals, as expected from the crystal structure. Although the sites of $Ni_{12}P_5$ differ to a much greater extent than those in Ni_2P, which are both tricapped trigonal prismatic, the difference in their electronic properties appears to be nevertheless smaller. The intensity ratio between the two signals should be four according to the relative occurrence of the two sites in the structure model of $Ni_{12}P_5$. The value found for the different samples containing $Ni_{12}P_5$ is 4 ± 0.5.

The particle sizes of the nickel phosphides supported on SiO_2 studied in this work were large enough to enable the identification of the nickel phosphide formed by XRD. In catalysis, however, one is interested in highly dispersed catalytic materials, and these often have XRD lines that are too broad to be observed. For such well-dispersed systems, the MAS NMR technique might offer the possibility of identifying small particles, because NMR spectroscopy is not restricted to materials with long-range order. The samples described in this work contain rather large particles, as indicated by the crystallite sizes given in Table 1. From the point of view of catalytic performance the particles are unfavorably large. However, this size made it possible to detect the different nickel phosphides by XRD and to correlate these results with the NMR spectra. This allowed us to collect NMR data that can be used in future studies for the characterization of metal phosphide particles, which are too small to be detected by XRD. Another technique that may be used to identify small particles is EXAFS. This technique requires synchrotron radiation, however, and is thus less generally applicable. Furthermore, the detection of different metal phosphide phases in one and the same sample can hardly be done by EXAFS. The MAS solid state NMR of ^{31}P thus proved to be very helpful in identifying the nickel phosphides formed.

NMR spectroscopy can be used to quantify the different species from the integrated signal intensities. However, problems arise when paramagnetic species are present, because the short relaxation times may cause loss of signal intensity during the detector's dead time (20). Furthermore, the proximity of a paramagnetic ion to a ^{31}P nucleus might broaden its NMR line beyond observability so that some fractions become NMR invisible. Therefore, we cannot exclude the possibility that phases exist in our supported samples that are XRD invisible because of their amorphous nature and NMR invisible because of their proximity to a paramagnetic center. As a consequence, we refrained for the moment from a quantitative analysis of the NMR data. Nevertheless, the quantitative analysis of paramagnetic species is possible when the spin echo mapping technique is applied, as shown by Tuel *et al.* for paramagnetic phosphate-based catalysts (56). Spin echo experiments of supported phosphide catalysts will be performed in the future.

5. CONCLUSIONS

We were able to prepare Ni_2P, Ni_3P, and $Ni_{12}P_5$ supported on SiO_2 by reducing an oxidic precursor by varying the reduction parameters and the P loading. In a first step Ni metal is formed that catalyzes the reduction of phosphate to a reactive P species. This species probably reacts through different intermediates; two of them could be identified as Ni_3P and $Ni_{12}P_5$. The support influences the reduction behavior very much since the reduction of the unsupported oxidic $NiP_{0.5}$ precursor yielded only Ni_2P and pure Ni_2P was not obtained from the supported $NiP_{0.5}$ precursor but only from the $NiP_{0.65}$ precursor under optimized reaction conditions. We were able to characterize the three different Ni phosphides by ^{31}P MAS NMR spectroscopy. The large NMR shifts are interpreted as Knight shifts and are easily distinguishable from shifts caused by diamagnetic phosphates. X-ray diffraction is not a technique suitable for identifying small metal phosphide crystallites supported on a carrier like SiO_2, but such small crystallites are important for catalysis. Since solid state NMR can be used to characterize amorphous or nanocrystalline metal phosphides, solid state NMR could be an alternative to EXAFS for characterizing supported metal phosphides.

REFERENCES

1. Kerfoot, Derek G. E., *in* "Ullmann's Encyclopedia of Industrial Chemistry. (Electronic Release)," 6th ed. Wiley-VCH, Weinheim, 1999.
2. Okamoto, Y., Nitta, Y., Imanaka, T., and Teranishi, S., *J. Catal.* **64**, 397 (1980).
3. Yoshida, S., Yamashita, H., Funabiki, T., and Yonezawa, T., *J. Chem. Soc. Faraday Trans. 1* **80**, 1435 (1984).
4. Yamashita, H., Yoshikawa, M., Funabiki, T., and Yoshida, S., *J. Chem. Soc. Faraday Trans. 1* **81**, 2485 (1985).
5. Lee, K. J., and Nash, P., *in* "Phase Diagrams of Binary Nickel Alloys" (P. Nash, Ed.), p. 235. ASM International, Materials Park, OH, 1991.
6. Shibata, M., and Masumoto, T., *in* "Preparation of Catalysts IV" (B. Delmon, P. Grange, P. A. Jacobs, and G. Poncelet, Eds.), p. 353. Elsevier, Amsterdam, 1987.
7. Brenner, A., and Riddell, G., *J. Res. Natl. Bur. Stand.* **39**, 385 (1947).
8. Ko, S.-H., Chou, T.-C., and Yang, T.-J., *Ind. Eng. Chem. Res.* **34**, 457 (1995).
9. Deng, J. F., Zhang, X. P., and Enze, M., *Appl. Catal.* **37**, 339 (1988).
10. Li, H. X., Wang, W. J., Li, H., and Deng, J. F., *J. Catal.* **194**, 211 (2000).
11. Deng, J. F., Chen, H. Y., Bao, X. H., and Muhler, M., *Appl. Surf. Sci.* **81**, 341 (1994).
12. Aronsson, B., Lundström, T., and Rundqvist, S., "Borides, Silicides and Phosphides—A Critical Review of Their Preparation, Properties and Crystal Chemistry." Methuen, London, 1965.
13. Gopalakrishnan, J., Pandey, S., and Rangan, K. K., *Chem. Mater.* **9**, 2113 (1997).
14. Sweeny, N. P., Rohrer, C. S., and Brown, O. W., *J. Am. Chem. Soc.* **80**, 799 (1958).
15. Nozaki, F., and Adachi, R., *J. Catal.* **40**, 166 (1975).
16. Nozaki, F., Kitoh, T., and Sodesawa, T., *J. Catal.* **62**, 286 (1980).
17. Robinson, W. R. A. M., van Gestel, J. N. M., Koranyi, T. I., Eijsbouts, S., van der Kraan, A. M., van Veen, J. A. R., and de Beer, V. H. J., *J. Catal.* **161**, 539 (1996).
18. Stinner, C., Prins, R., and Weber, Th., *J. Catal.* **202**, 187 (2001).
19. Mangnus, P. J., van Veen, J. A. R., Eijsbouts, S., de Beer, V. H. J., and Moulijn, J. A., *Appl. Catal.* **61**, 99 (1990).
20. Kraus, H., and Prins, R., *J. Catal.* **170**, 20 (1997).
21. Nolze, G., and Kraus, W., *Powder Diffr.* **13**, 256 (1998).
22. Larsson, E., *Ark. Kemi* **23**, 335 (1965).
23. Herzfeld, J., and Berger, A. E., *J. Chem. Phys.* **73**, 6021 (1980).
24. Massiot, D., Thiele, H., and Germanus, A., *Bruker Rep.* **140**, 43 (1994).
25. Bassett, H., and Bedwell, W. L., *J. Chem. Soc.* 871 (1933).
26. Eichele, K., and Wasylishen, R. E., *J. Phys. Chem.* **98**, 3108 (1994).
27. Gunter, G. C., Craciun, R., Tam, M. S., Jackson, J. E., and Miller, D. J., *J. Catal.* **164**, 207 (1996).
28. Krawietz, T. R., Lin, P., Lotterhos, K. E., Torres, P. D., Barich, D. H., Clearfield, A., and Haw, J. F., *J. Am. Chem. Soc.* **120**, 8502 (1998).
29. Jones, A., and McNicol, B., "Temperature-Programmed Reduction for Solid Materials Characterization." Dekker, New York, 1986.
30. El Belghiti, A. A., Boukhari, A., and Holt, E. M., *J. Alloys Compd.* **188**, 128 (1992).
31. Louis, C., Cheng, Z. X., and Che, M., *J. Phys. Chem.* **97**, 5703 (1993).
32. Baiker, A., and Maciejewski, M., *J. Chem. Soc. Faraday Trans. 1* **80**, 2331 (1984).
33. Verhaak, M. J. F. M., van Dillen, A. J., and Geus, J. W., *Appl. Catal. A* **105**, 251 (1993).
34. Burattin, P., Che, M., and Louis, C., *J. Phys. Chem. B* **104**, 10482 (2000).
35. Myers, C. E., and Conti, T. J., *J. Electrochem. Soc.* **132**, 454 (1985).
36. Ryndin, Y. A., Candy, J. P., Didillon, B., Savary, L., and Basset, J. M., *J. Catal.* **198**, 103 (2001).
37. Konstantinow, N., *Z. Anorg. Chem.* **60**, 405 (1908).
38. Nowotny, H., and Henglein, E., *Z. Phys. Chem. B* **40**, 281 (1938).
39. Saini, G. S., Calvert, L. D., and Taylor, J. B., *Can. J. Chem.* **42**, 1511 (1964).
40. Pittermann, U., and Ripper, S., *Phys. Status Solidi A* **93**, 131 (1986).
41. Rundqvist, S., and Larsson, E., *Acta Chem. Scand.* **13**, 551 (1959).
42. Rundqvist, S., Hassler, E., and Lundvik, L., *Acta Chem. Scand.* **16**, 242 (1962).
43. von Schnering, H. G., and Hönle, W., *in* "Encyclopedia of Inorganic Chemistry" (K. R. Bruce, Ed.), vol. 6, p. 3106. Wiley, Chichester, 1994.
44. Corbridge, D. E. C., "Phosphorus 2000—Chemistry, Biochemistry & Technology." Elsevier, Amsterdam, 2000.
45. Ripley, R. L., *J. Less-Common Met.* **4**, 496 (1962).
46. Shirotani, I., Takahashi, E., Mukai, N., Nozawa, K., Kinoshita, M., Yagi, T., Suzuki, K., Enoki, T., and Hino, S., *Jpn. J. Appl. Phys. Part 1* **32**, 294 (1993).
47. Zeppenfeld, K., and Jeitschko, W., *J. Phys. Chem. Solids* **54**, 1527 (1993).
48. Knight, W. D., and Kobayashi, S., *in* "Encyclopedia of Nuclear Magnetic Resonance" (D. M. Grant and R. K. Harris, Eds.), p. 2672. Wiley, Chichester, 1996.
49. Drain, L. E., *Proc. Phys. Soc.* **80**, 1380 (1962).
50. Andrew, E. R., Hinshaw, W. S., and Tiffen, R. S., *Phys. Lett. A* **46**, 57 (1973).
51. Nissan, R. A., and Vanderah, T. A., *J. Phys. Chem. Solids* **50**, 347 (1989).
52. Lathrop, D., Franke, D., Maxwell, R., Tepe, T., Flesher, R., Zhang, Z., and Eckert, H., *Solid State Nucl. Magn. Reson.* **1**, 73 (1992).
53. Tomaselli, M., deGraw, D., Yarger, J. L., Augustine, M. P., and Pines, A., *Phys. Rev. B* **58**, 8627 (1998).
54. Schmedt auf der Günne, J., Kaczmarek, S., van Wüllen, L., Eckert, H., Paschke, D., Foecker, A. J., and Jeitschko, W., *J. Solid State Chem.* **147**, 341 (1999).
55. Furo, I., Bakonyi, I., Tompa, K., Zsoldos, E., Heinmaa, I., Alla, M., and Lippmaa, E., *J. Phys. Condens. Matter* **2**, 4217 (1990).
56. Tuel, A., Canesson, L., and Volta, J. C., *Colloid Surf. A* **158**, 97 (1999).